Design of a Total Energy Control Autopilot Using Constrained Parameter Optimization

Christopher Voth*
Martin Marietta, Denver, Colorado 80201
and
Uy-Loi Ly†
University of Washington, Seattle, Washington 98195

The application of a multivariable control design method based on constrained parameter optimization to the design of a multiloop aircraft flight control system is described. Specifically, the design method is applied to the direct synthesis of a multivariable "inner-loop" feedback control system based on total energy control principles. The design procedure offers a structured approach for the determination of a set of controller gains that meet design specifications in closed-loop stability, command tracking performance, disturbance rejection, and limits on control activities. The presented approach may be applied to a broader class of multiloop flight control systems. Direct tradeoffs between many real design goals are rendered systematic by this method following proper formulation of the design objectives and constraints. Performance characteristics of the optimized design have been improved over the current autopilot design on the B737-100 Transport Systems Research Vehicle at the landing approach and cruise conditions, particularly in the areas of closed-loop damping and control activity in the presence of turbulence.

Nomenclature

a = command filter lag, s^{-1}
A_C = controller state matrix
A_p = plant state matrix
B_C = controller input gain matrix
B_p = plant control input distribution matrix
C_C = controller state to output gain matrix
C_p = plant state to output distribution matrix
D = drag, lbs
D_C = controller direct feedthrough gain matrix
D_p = plant control to output distribution matrix
E = total energy, ft-lbs
$\dot{E}$ = total energy rate, ft-lbs/s
e = exponential function
G_{yw} = closed-loop system transfer matrix between inputs $w(s)$ and outputs $y(s)$
g = gravitational constant, fps^2
h = altitude, ft
I = identity matrix
J = design objective function
j = $\sqrt{-1}$
K_{CAS} = gain schedule based on calibrated airspeed
K_{EI} = integral gain on energy distribution rate
K_{EP} = proportional gain on energy distribution rate
K_{GW} = gain schedule based on gross weight
K_q = pitch rate feedback gain
K_{TI} = integral gain on energy rate
K_{TP} = proportional gain on energy rate
K_θ = pitch angle feedback gain
k_1 = static gain between aircraft velocity and velocity command
k_2 = static gain between aircraft velocity and flight path command
m = mass, slugs
N_o = number of output covariance constraints
N_p = total number of design conditions
n = order of the closed-loop system
n_{zcg} = normal acceleration at the aircraft center of gravity, g
Q = positive semi-definite criterion output penalty weighting matrix
q = pitch rate, deg/s
R = positive semi-definite control penalty weighting matrix
s = Laplace variable, s^{-1}
T = thrust, lbs
T_{req} = thrust required, lbs
t = time
t_f = terminal time, s
u_c = controller input vector
u_g = longitudinal wind component
u_p = plant control input vector
V = aircraft inertial velocity, fps
$\dot{V}$ = acceleration, fps^2
V_c^* = achievable velocity response to simultaneous velocity and flight-path commands
W_{pi} = weighting assigned to performance index J_i
w_g = transverse wind component
w_p = plant disturbance/command input vector
x_C = controller state vector
x_{IE} = integral of normalized total energy rate
x_{IL} = integral of normalized total energy distribution rate
x_p = plant state vector
x_{ug} = state of longitudinal Dryden turbulence model
x_{Vc} = integral of acceleration command, fps
x_{wg1}, x_{wg2} = states of transverse Dryden turbulence model
$x_{\delta e}$ = elevator actuator state
$x_{\delta th1}, x_{\delta th2}$ = throttle actuator states
y_C = controller output vector
y_p = plant output vector
α = angle of attack, deg
β = destabilization factor, s^{-1}
γ = flight-path angle, rad
Γ_p = plant disturbance/command input distribution matrix

Received March 13, 1990; revision received June 21, 1990; accepted for publication July 29, 1990.

*Technical Staff, Space Systems Division, M.S. 4372. Member AIAA.
†Assistant Professor, Department of Aeronautics and Astronautics. Member AIAA.

δ = control perturbation
ΔT_{req} = incremental thrust required, lbs
ζ = damping ratio
θ = pitch angle, deg
κ = prespecified scalar variable
σ = real part of eigenvalue
σ_u = rms intensity of longitudinal turbulence, fps
σ_w = rms intensity of transverse turbulence, fps
σ_{yp} = plant output rms response
ω = frequency, rad/s
ω_n = magnitude of eigenvalue, rad/s
Ω_p = plant disturbance/command to output distribution matrix

Subscripts

C = controller model
c = command input
ec = elevator command
lbt = pounds of thrust
lbw = pounds of weight
p = plant model
Tc = thrust command
thc = throttle command
ϵ = error

Superscripts

i = ith plant model
T = transpose
$E[\,]$ = expected value
$\bar{\sigma}$ = maximum singular value
sup = supremum

Introduction

RECENT developments in control system design techniques have focused on the improvement of controller performance and robustness to uncertainties in the plant model. Modern control system design methods such as linear quadratic Gaussian/loop transfer recovery (LQG/LTR), H^∞, and μ synthesis can provide controllers with high levels of performance and robustness.[1-3] However, the controllers obtained by using these techniques are of high order. The number of controller states is usually greater than or equal to the number of states in the plant model. Controller order must be reduced subsequently for the final design implementation. Alternative methods based on output feedback are available[4-6] to address some of the aforementioned issues. In particular, the design algorithm developed in Ref. 6 provides a convenient framework for designing optimal low-order controllers. Recent extension of this method[7] and the use of constrained nonlinear optimization[8] enable designers to address requirements, such as eigenvalue damping and covariance constraints, that are not easily expressible in terms of an objective function based on quadratic performance indices.

Traditionally, classical design procedures based on single-loop closure and root locus have been applied to the design of multiloop control systems. Designs obtained with conventional methods can have low performance and robustness to plant model uncertainties. Tradeoffs between performance and robustness requirements are far from simple and can be time consuming, especially when the designers lack appropriate past design experiences. Furthermore, the classical design procedures often overlook, due to their single-input/single-output nature, the intrinsic multivariable aspects of the design problem. As a result, the control system may not contain appropriate crossfeed among individual feedback loops, limiting the maximum achievable performance.

Complexities in present automatic flight control systems (AFCS) for commercial transport aircraft are generally associated with the lack of suitable control design integration, i.e., crossfeed among different control paths. Recent work by Lambregts[9-11] on the NASA B737-100 Transport System Research Vehicle (TSRV), on improving the operation of the AFCS, has led to the development of a total energy control system (TECS) for an integrated autothrottle/autopilot design. The design philosophy incorporates fundamental aspects of the aircraft dynamics into the formulation of a *multiloop* controller structure. This innovative design approach has led to a controller structure that contains key cross-coupling between the elevator and throttle control loops for improved performance. Selection of the feedback gains was still performed using classical design procedures.[9-14] To satisfy multiple design requirements, such as closed-loop stability, control and command bandwidths, control activities in the presence of turbulence, and design robustness to modeling uncertainties, the one-loop-at-a-time iterative procedure can be time-consuming.

Potentially, application of multivariable control design techniques could provide a systematic approach to the solution for a set of feedback gains that achieve simultaneously design performance and robustness to plant model uncertainties. One such approach is provided by the unified design algorithm for robust low-order controllers[6] using constrained parameter optimization implemented in the computer program SANDY.[7] It has found numerous applications in flight controls[15-17] and control of flexible mechanical systems.[18] This paper demonstrates the application of the design algorithm to the synthesis of an integrated autothrottle/autopilot "inner" structure based on the TECS design philosophy.

The main objective of this work is the formulation of an optimal control problem addressing the same design objectives that are achieved using classical design approaches; in this case, the design solution is based on direct constrained optimization. With this formulation, a systematic approach is developed allowing the designers to achieve multiple design objectives, such as damping of system modes, shaping of loop frequency responses, disturbance rejection, command tracking, and robustness to modeling uncertainties. Using this design technique, feedback gains have been obtained for the integrated autothrottle/autopilot design on the TSRV at two flight conditions. Linear analysis indicates that the design procedure using constrained optimization yields comparable and improved results in closed-loop stability, aircraft response and control activities to turbulence, and robustness in terms of single-input/single-output gain and phase margins.

Design Objectives of Integrated Automatic Flight Control System

A series of design objectives were formulated for design of an integrated flight control system. These objectives are enumerated here.[9-11]

1) Integration of all vertical control modes into a single control law concept. The system should be designed around a fixed inner-loop configuration with outer-loop control modes generating signals compatible with the inner-loop command inputs.

2) Minimization of transient errors due to cross-coupling between commanded inputs in the inner-loop structure.

3) Elimination of functional overlaps in the AFCS design.

4) Protection against exceeding aircraft performance and structural limits by providing an intelligent hierarchy in control system modes.

5) Provision for overshoot free responses to step command inputs.

6) Augmentation of closed-loop damping of dominant poles to an acceptable level.

7) Minimization of control activities in response to turbulence in accordance with meeting flight-path and speed tracking requirements at each flight condition.

Review of Total Energy Control Concept

Numerous variations of energy compensation techniques have been investigated for improving the simultaneous opera-

tion of the autothrottle and autopilot designs. One formulation of the energy compensation technique[9-11] is to develop the engine thrust command as a function of the aircraft total energy rate, while the elevator command is expressed as a function of the kinetic and potential energy distribution rate. Key equations governing the total energy control concept were developed in Refs. 9-11. They are included here for completeness and to define the structure of the control system used in the constrained parameter optimization that follows.

The total energy E of the aircraft treated as a point mass is given by

$$E = \tfrac{1}{2}mV^2 + mgh \tag{1}$$

The total energy rate $\dot{E}$ is found by differentiating E in Eq. (1) with respect to time as

$$\dot{E} \approx mgV[(\dot{V}/g) + \gamma] \tag{2}$$

for the small flight-path angle (FPA) γ (rad) and assuming m constant. If we write the equation for the thrust required from the equations of motion along the flight path, we have

$$T_{\text{req}} = mg[(\dot{V}/g) + \gamma)] + D \tag{3}$$

Assuming that the initial thrust is trimmed against drag and the variations in drag are generally slow, then it follows that the short-term thrust requirement for a desired level of total energy rate is obtained from the acceleration and FPA quantities as

$$\Delta T_{\text{req}} = \dot{E}/V = mg[(\dot{V}/g) + \gamma] \tag{4}$$

This implies that the aircraft total energy can be regulated directly using thrust control. However, the distribution between kinetic and potential energies cannot be controlled effectively with the throttles. To distribute the total energy rate between flight path and acceleration as desired, elevator control must be used. The elevator primarily provides control of angle of attack and, thus, lift, while contributing little to the aircraft total drag, thereby having little effect on the total energy rate.

Using proportional and integral control on the total energy rate and energy rate distribution, we develop the thrust and elevator commands as

$$\delta_{\text{Tc}} = mg\left(K_{TP} + \frac{K_{TI}}{s}\right)\left(\frac{\dot{V}_\epsilon}{g} + \gamma_\epsilon\right) \tag{5}$$

$$\delta_{\text{ec}} = \left(K_{EP} + \frac{K_{EI}}{s}\right)\left(\frac{\dot{V}_\epsilon}{g} - \gamma_\epsilon\right) \tag{6}$$

where $\gamma_\epsilon = \gamma - \gamma_c$ and $\dot{V}_\epsilon = \dot{V} - \dot{V}_c$ represent the errors of flight-path angle γ and acceleration $\dot{V}$ from the commanded values γ_c and $\dot{V}_c$, respectively. The parameters K_{TP}, K_{TI}, K_{EP}, and K_{EI} are the proportional and integral feedback gains to thrust and elevator controls, respectively. The basic implementation of this system is shown in Fig. 1. Notice that proportional paths on the flight path γ_c and acceleration $\dot{V}_c$ commands [in Eqs. (5) and (6)] have been left out of the current implementation. It was found that direct feedback of the commanded inputs to the controls would produce undesirable overshoots. However, such a problem can be resolved with proper feedforward control.

Analysis of Current Total Energy Control Structure

A careful study of the TECS structure and its characteristics is crucial to the formulation of an optimal control design procedure. Table 1 shows the inner loop and pitch damper gain selection for the current design implementation on the NASA TSRV.[12-14] The gains K_θ and K_q provide feedback of

Table 1 Current TECS inner-loop and pitch damper gains

K_{TI}	K_{EI}	K_{TP}	K_{EP}	K_θ	K_q
0.4	2.52	0.0	3.36	6.0	4.0

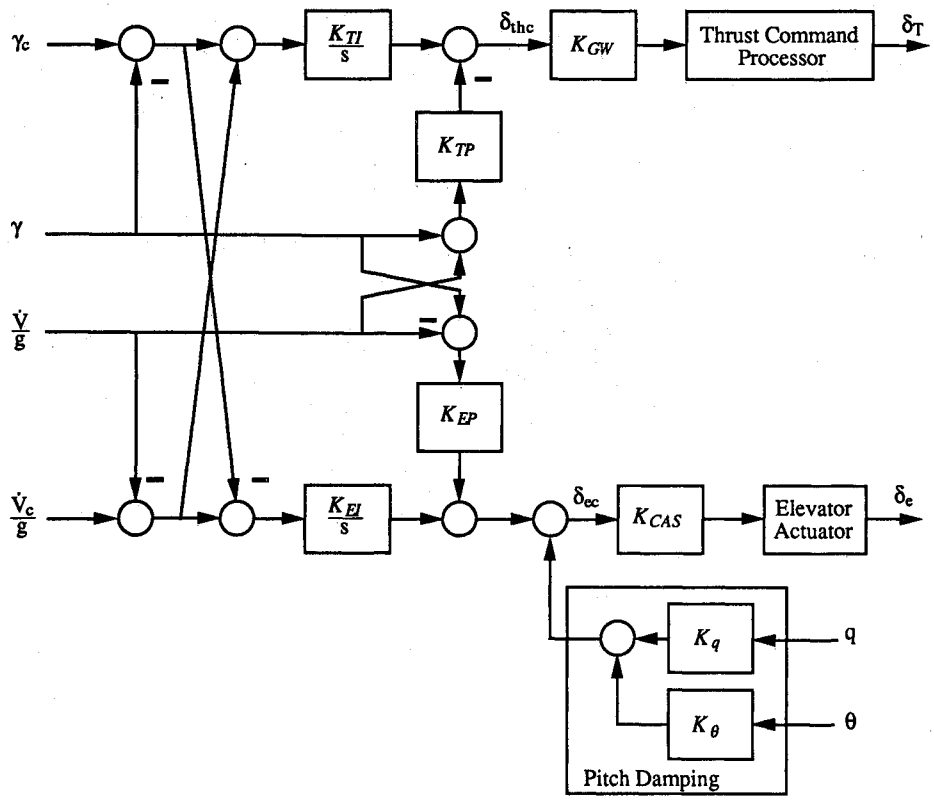

Fig. 1 Basic total energy control system.

pitch attiude and pitch rate for stabilization of the aircraft longitudinal rigid-body modes. Notice that the gain K_{TP} was set to zero, thus eliminating the proportional feedback path to the throttles. Classical analysis indicates that this feedback gain is not necessarily for closed-loop stability. Furthermore, by eliminating direct feedback to the throttle, the broken-loop control bandwidth and throttle activity are reduced. Actually this restriction on K_{TP} is not needed as demonstrated in the optimal TECS design. The additional degree of freedom provided by the gain K_{TP} can be used to improve further the stability of the phugoid and short-period modes, and to achieve better command tracking performance without increasing control activity response to turbulence.

The integral gains K_{TI} and K_{EI} were chosen to be approximately equal so as to obtain equal bandwidths in both the γ_ϵ and $\dot{V}_\epsilon/g$ feedback paths. Gain scheduling of the control system to different flight conditions is achieved through the gains K_{CAS} and K_{GW} in the elevator and throttle loop, respectively (Fig. 1). The gain schedules are a function of calibrated airspeed (CAS) in knots and gross weight (GW) in pounds as

$$K_{CAS} = (200/\mathrm{CAS})^2 \tag{7}$$

$$K_{GW} = mg \tag{8}$$

With these gain schedules, the control law will be nonlinear and time-varying when implemented.

The TECS structure as shown in Fig. 1 introduces an uncontrollable pole at the origin in the closed-loop system. This results from additional integration of the aircraft acceleration variable $\dot{V}(t)$ in the control system. This means that the design provides only one integral action effective on the flight-path response and not on velocity. Integral control of the velocity variable can be obtained only by feedback of the velocity variable, as in an outer-loop control design for a speed-hold-type autopilot. Design of outer loops for different autopilot modes is left for a future study. This paper primarily addresses the control design problem of the inner-loop gains using a procedure based on constrained optimization.

In the next section, we describe briefly key elements in the setup of a design procedure based on constrained optimization.

Optimal Design Procedure

The design method is documented in Refs. 6 and 7. In this section, we summarize the system formulation and performance index definition required for the design algorithm.

Formulation of Plant Synthesis and Controller Models

The aircraft dynamic model is usually linearized about some equilibrium conditions. The linearized plant model at the ith condition ($i = 1, N_p$) is a continuous linear time-invariant model of the form

$$\dot{x}_p^i(t) = A_p^i x_p^i(t) + B_p^i u_p^i(t) + \Gamma_p^i w_p^i(t) \tag{9}$$

$$y_p^i(t) = C_p^i x_p^i(t) + D_p^i u_p^i(t) + \Omega_p^i w_p^i(t) \tag{10}$$

where A_p^i, B_p^i, C_p^i, D_p^i, Γ_p^i, and Ω_p^i are state model matrices associated with the aircraft dynamics, actuator dynamics, and disturbance filter models.

Application of the design method requires an a priori defined structure for both the feedback and feedforward controllers. A typical feedback/feedforward controller has the form

$$\dot{x}_C(t) = A_C x_C(t) + B_C u_C(t) \tag{11}$$

$$y_C(t) = C_C x_C(t) + D_C u_C(t) \tag{12}$$

where the matrices A_C, B_C, C_C, and D_C provide the dynamic compensation (i.e., proportional, integral, derivative, leads, lags, etc.) on the feedback sensor quantities and commanded outputs; both are represented in the input vector $u_C(t)$. For example, $u_C(t) = \{q, \theta, \gamma, \dot{V}, \gamma_c, \dot{V}_c\}$. The controller output vector $y_C(t)$ contains feedback controls and output variables that are expressed as a linear combination of controller states $x_C(t)$ and controller inputs $u_C(t)$; e.g., $y_C(t) = \{\delta_{\mathrm{thc}}, \delta_{\mathrm{ec}}, V_c^*\}$. Most linear time-invariant controllers can be put into this form with individual feedback gains appearing in the elements of the state matrices A_C, B_C, C_C, and D_C. Note that a closed-loop system is formed by connecting 1) the plant outputs $y_p^i(t)$ to the inputs $u_C(t)$ of the controller model, and 2) the controller outputs $y_C(t)$ to the inputs $u_p^i(t)$ of the plant model.

Formulation of Objective Function and Design Constraints

Typical performance measures in optimal control are quadratic penalties on closed-loop system output and control responses to disturbances. Three types of random disturbances are considered in the design algorithm: initial conditions, impulse inputs, and white noise inputs. Depending on the types of disturbances, different formulations of the performance index are used. A performance index involving initial conditions or impulse inputs has the form

$$J = \lim_{t_f \to \infty} \frac{1}{2} \sum_{i=1}^{N_p} W_{pi} \int_0^{t_f} e^{2\beta t} E[y_p^{iT}(t) Q^i y_p^i(t) + u_p^{iT}(t) R^i u_p^i(t)]\, dt \tag{13}$$

and for white-noise inputs, the performance index is

$$J = \lim_{t_f \to \infty} \frac{1}{2t_f} \sum_{i=1}^{N_p} W_{pi} \int_0^{t_f} e^{2\beta t} E[y_p^{iT}(t) Q^i y_p^i(t) + u_p^{iT}(t) R^i u_p^i(t)]\, dt \tag{14}$$

where $y_p^i(t)$ and $u_p^i(t)$ are the criterion outputs and the control inputs, respectively, evaluated at the ith plant condition. The parameter is used to ensure that, when a steady-state optimal solution has been reached, the closed-loop system eigenvalues of the controllable modes will have real parts less than $-\beta$. The formulation of the outputs $y_p^i(t)$ in Eq. (10) is general and can be defined to include plant states $x_p^i(t)$, controller states $x_C(t)$, and controller inputs $u_C(t)$. The plant states $x_p^i(t)$ are modeled in the criterion outputs $y_p^i(t)$ by letting $C_p^i = I$, $D_p^i = 0$, and $\Omega_p^i = 0$. The controller states $x_C(t)$ and the controller inputs $u_C(t)$ are modeled through the term D_p^i in Eq. (10) and with $u_p^i(t) = y_C(t)$ established in the feedback connection.

The performance index J given in Eqs. (13) and (14) enables designers to incorporate classical measures of design robustness or sensitivity into plant modeling uncertainties of the following types:

1) Gain and phase margins in the control and sensor paths.

2) Rolloff in broken-loop frequency responses of the control and sensor feedback paths.

3) Sensitivity of the closed-loop eigenvalues and closed-loop performance measures to perturbation of the plant model parameters.

The first and second items are useful measures of robustness to unmodeled dynamics. Item 3 is a measure of robustness to uncertainties in the coefficients of the plant model.

As seen in Eqs. (13) and (14), the design algorithm incorporates quadratic penalties of closed-loop system responses at different plant conditions into a single objective function. Design to multiple plant conditions ($i = 1, N_p$) allows the inclusion of robustness measures of type 3 directly into the design objective. Design to robustness measures of types 1 and 2 can also be handled through the use of frequency-weighted performance functions and H^∞ bounds on selected system transfer function matrices.[3,19]

Design gains and selected parameters within the controller state matrices A_C, B_C, C_C, and D_C are optimized via a nonlinear programming technique developed in NPSOL,[8] such that

the performance index J in Eq. (13) or (14) is minimized. The performance index is evaluated to a finite terminal time t_f during the initial optimization. Efficient algorithms to evaluate the performance index $J(t_f)$ and its gradients with respect to the design parameters were developed[6] that are comparable to those in the evaluation of the steady-state performance index (i.e., based on Lyapunov equations). The terminal time t_f is subsequently increased after each successful convergence in order to recover the steady-state solution. This gradual process of recovering the steady-state solution ensures that the final optimal solution will be a stabilizing one. Experiences gathered so far appear to justify the use of a performance index based on finite terminal time. This procedure avoids the difficulties encountered by conventional methods based on the Lyapunov equation for the steady-state covariance responses, requiring special provision to handle the case when the controller design becomes destabilizing during the search.

Design for command following/tracking is done by formulating synthesis models and performance indices that penalize transient responses between the actual and commanded outputs. Commanded outputs (e.g., filtered step, ramp, sinusoidal functions) are generated from a feedforward controller model using a combination of initial conditions and impulse inputs.

Design requirements that cannot be handled easily through a quadratic performance index are enforced through linear constraints, nonlinear constraints, and direct bounds on the design parameters. Nonlinear constraints on closed-loop stability, performance, and robustness are defined as follows.

1) Closed-loop damping of selected eigenvalues:

$$\zeta_i \geq \zeta_{i\min}, \qquad i = 1,n \tag{15}$$

and

$$\sigma_i \leq \sigma_{i\max}, \qquad i = 1,n \tag{16}$$

2) Closed-loop mean-square responses:

$$\lim_{t_f \to \infty} E[y_{pi}^2(t_f)] \leq \sigma_{ypi\max}^2, \qquad i = 1,N_o \tag{17}$$

3) Desired H^∞-norm bounds on closed-loop performance variables:

$$\|G_{yw}(j\omega)\|_\infty \leq \kappa \tag{18}$$

where

$$\|G_{yw}(j\omega)\|_\infty = \sup_\omega \bar{\sigma}[G_{yw}(j\omega)]$$

Design Example

To examine the total energy system design using constrained parameter optimization, the NASA B-737-100 TSRV aircraft was used.[9-14] Linearized aircraft longitudinal models are obtained for two flight conditions (Table 2): a landing approach condition (FLT1) and a cruise condition (FLT2). The aircraft rigid-body models are subsequently augmented with actuator dynamics and Dryden turbulence models to yield a model for control-law synthesis in the form of Eqs. (9) and (10) with state vector $x_p(t) = \{V, \alpha, q, \theta, x_{\delta th1}, x_{\delta th2}, x_{\delta e}, x_{ug}, x_{wg1}, x_{wgh2}\}^T$, control input vector $u_p(t) = \{\delta_{thc}, \delta_{ec}\}$, disturbance/command input vector $w_p(t) = \{u_g, w_g, \gamma_c, \dot{V}_c\}$, and output vector $y_p(t) = \{q, \theta, \gamma, \dot{V}, \gamma_c, \dot{V}_c, n_{zcg}\}^T$.

Table 2 TSRV B737-100 flight conditions

	Altitude, ft	Weight, lb	CAS, kt	Flaps, deg	FPA, deg	Gear
FLT1	1,500	80,000	120	40	−3	Down
FLT2	25,000	80,000	450	0	0	Up

The basic TECS feedback controller with pitch damping (Fig. 1) can be represented in the following state-space form:

$$\begin{bmatrix} \dot{x}_{IE} \\ \dot{x}_{IL} \\ \dot{x}_{Vc} \end{bmatrix} = \begin{bmatrix} 0 & 0 & 0 \\ 0 & 0 & 0 \\ 0 & 0 & 0 \end{bmatrix} \begin{bmatrix} x_{IE} \\ x_{IL} \\ x_{Vc} \end{bmatrix} + \begin{bmatrix} 0 & 0 & -1 & -1 & 1 & 1 \\ 0 & 0 & 1 & -1/g & -1 & 1/g \\ 0 & 0 & 0 & 0 & 0 & 1 \end{bmatrix} \begin{bmatrix} q \\ \theta \\ \gamma \\ \dot{V} \\ \gamma_c \\ \dot{V}_c \end{bmatrix} \tag{19a}$$

$$\begin{bmatrix} \delta_{thc} \\ \delta_{ec} \\ V_c^* \end{bmatrix} = \begin{bmatrix} K_{TI} & 0 & 0 \\ 0 & K_{EI} & 0 \\ 0 & 0 & k_1 \end{bmatrix} \begin{bmatrix} x_{IE} \\ x_{IL} \\ x_{Vc} \end{bmatrix} + \begin{bmatrix} 0 & 0 & -K_{TP} & -K_{TP}/g & 0 & 0 \\ K_q & K_\theta & K_{EP} & -K_{EP}/g & 0 & 0 \\ 0 & 0 & 0 & 0 & k_2 & 0 \end{bmatrix} \begin{bmatrix} q \\ \theta \\ \gamma \\ \dot{V} \\ \gamma_c \\ \dot{V}_c \end{bmatrix} \tag{19b}$$

Proportional and integral gains K_{TP}, K_{EP}, K_{TI}, and K_{EI} along with the pitch damper gains K_q and K_θ and the additional gains k_1 and k_2 are design parameters in the controller state matrices.

Arrival at a final design using constrained optimization involves compromise among different design performance goals. For example, for the landing approach flight condition FLT1, the following design objectives were used.

1) Stability of the closed-loop eigenvalues:

a) Real parts of all the eigenvalues are restricted to be less than zero, i.e.,

$$\sigma_i < 0, \qquad i = 1,n \tag{20}$$

b) Damping ratios of all the eigenvalues are restricted to be greater than 0.7, i.e.,

$$\zeta_i \geq 0.7, \qquad i = 1,n \tag{21}$$

2) Mean-square responses of control activities to clear air Dryden turbulence of $\sigma_u = 6.6$ fps and $\sigma_w = 6.3$ fps,

$$E[\delta_{thc}^2] \leq 0.74 \times 10^{-3} \text{ (lbt/lbw)}^2 \tag{22}$$

$$E[\delta_{ec}^2] \leq 2.127 \text{ deg}^2 \tag{23}$$

3) Command frequency response bandwidths and command tracking performance:

$$J_1 = \lim_{t_f \to \infty} \frac{1}{2} \int_0^{t_f} E\{Q_1[\gamma(t) - \gamma_c(t)]^2 + Q_2[V(t) - V_c^*(t)]^2\}\, dt \tag{24}$$

The performance index J_1 is evaluated for parameterized random filtered step commands $\bar{V}_c(t)$ and $\gamma_c(t)$ with $\bar{V}_c(t) = V_{co} a e^{-at} \mu(t)$ and $\gamma_c(t) = \gamma_{co}(1 - e^{-at})\mu(t)$, where $\mu(t)$ is the unit step function. The parameter a determines the bandwidths of both the acceleration and the flight-path commands. In this design case, we use $a = 1.2$ rad/s, a typical value for flight-path and velocity command bandwidths. The variables

V_{co} and γ_{co} are random parameters with zero means and covariances $E[V_{co}^2] = \sigma_{Vc}^2 = 1.0$ fps^2 and $E[\gamma_{co}^2] = \sigma_{\gamma c}^2 = 1.0$ deg^2. Note that the TECS control law (Fig. 1) is not of type 1 in velocity V. In steady state, the aircraft velocity $V(t)$ does not settle to the commanded value $V_c(t)$. Thus, we introduce the variable $V_c^*(t)$ in Eq. (24). It is defined in Eqs. (19) as a linear combination of the commanded velocity $V_c(t)$ and flight-path angle $\gamma_c(t)$; i.e., $V_c^*(t) = k_1 V_c(t) + k_2 \gamma_c(t)$. The parameter k_1 depicts the achieved level of commanded velocity in steady state and $k_1 < 1$ for a type 0 system. The parameter k_2 represents the amount of cross-coupling between the flight-path command $\gamma_c(t)$ and aircraft steady-state velocity $V(t)$. Either parameter k_1 and/or k_2 can be set to lie within some desired values using direct bound constraints. For our design, the parameter k_1 was unconstrained and an inequality constraint $-1 \le k_2 \le 1$ was defined on the parameter k_2 to ensure that, for 1-deg FPA command $\gamma_c(t)$, the change in aircraft steady-state velocity is less than 1 fps in magnitude. The parameters k_1 and k_2 are determined during the optimization such that bound constraints on k_1 and k_2 are satisfied, and the term $V(t) - V_c^*(t)$ in the integrand of J_1 vanishes in the steady state. The resulting optimized values of k_1 and k_2 will vary with flight conditions. The weighting parameters Q_1 and Q_2 are selected iteratively until the desired tracking performance and command bandwidths of the respective outputs are achieved. If the bandwidth for a particular command loop is too low and corresponding tracking performance is poor, increasing the penalty parameter Q_i ($i = 1,2$) will result systematically in higher bandwidth and improved tracking performance of the respective command loop.

4) Broken-loop crossover frequencies in the control paths:

a) *Throttle control loop*. Control bandwidth of the throttle loop is defined by using the performance index

$$J_2 = \lim_{t_f \to \infty} \frac{1}{2} E[R_1 \delta_{thc}^2(t_f)] \tag{25}$$

The performance index J_2 is evaluated to a high-pass noise input in the thrust command loop. Cutoff frequency of the high-pass filter is set approximately equal to the desired broken-loop throttle control bandwidth (i.e., $\omega_{thc} = 0.2$ rad/s). Frequency shaping of the input to the thrust command ensures that only control responses at high frequencies are penalized in J_2.

b) *Elevator control loop*. Similarly, control bandwidth of the elevator loop is defined by

$$J_3 = \lim_{t_f \to \infty} \frac{1}{2} E[R_2 \delta_{ec}^2(t_f)] \tag{26}$$

In this case, the performance index J_3 is evaluated to a high-pass noise input in the elevator command loop. Cutoff frequency of the high-pass filter is set approximately equal to the desired broken-loop elevator control bandwidth (i.e., $\omega_{ec} = 2.0$ rad/s). Notice that the elevator control has a higher bandwidth than the throttle control. Weighting parameters R_i ($i = 1,2$) in Eqs. (25) and (26) are selected iteratively until the desired bandwidths of the respective control loops are achieved. If the crossover frequency of a particular control loop is too high, then a higher penalty R_i ($i = 1,2$) should be tried.

After individual design requirements have been established, as in Eqs. (20–26), they are then put into the framework of the optimal design procedure. The design gains K_q, K_θ, K_{TP}, K_{EP}, K_{TI}, K_{EI}, k_1, and k_2 of the controller are then optimized with respect to a single quadratic performance index J of the form

$$J = \sum_{i=1}^{3} W_{pi} J_i \tag{27}$$

subject to the constraints of Eqs. (20–23), where J_i ($i = 1,3$) are defined in Eqs. (24–26). When successful convergence to a local minimum is obtained, the constraints and performance requirements are generally satisfied. This local minimum solution therefore provides a satisfactory set of design gains. To examine whether different local minima exist, one can restart the design optimization with significantly different initial design guesses.

The preceding procedure will give values of the controller design parameters that satisfy design requirements at one flight condition. Gain scheduling of the design at other flight conditions is usually required for optimum performance and may be achieved in one of three ways:

1) Design controller gains for individual flight conditions. The gain schedule is applied to all controller gains, and some form of curve-fitting with respect to airplane parameters such as CAS and GW is required in the implementation.

2) Design all controller gains for a nominal flight condition. Redesign at other flight conditions based on gain scheduling a subset of controller gains.

3) Preselect a gain schedule in each of the control or sensor paths. Design remaining controller parameters to satisfy design requirements with the selected gain schedule over the entire set of design conditions simultaneously.

The first method is straightforward and basically involves doing a separate design for each flight condition. However, this may result in a gain schedule that is too cumbersome to implement. In the TECS inner-loop structure (Fig. 1), this method would require scheduling of six separate feedback gains. A more practical approach is to select a few gains in the controller that are to be gain scheduled. These gains are often introduced at the control input paths to provide compensation for changes in control effectiveness. The procedure in the second method begins with a set of gains optimized at a nominal flight condition perceived to be the most important. Then the gain schedule is determined by optimizing only a selected subset of gains to other flight conditions, leaving the remaining controller gains fixed at nominal values. This is a preferred approach since it provides insights into the level of improvement a gain schedule can offer with the selected degrees of freedom. The third approach is not desirable, since it sets the gain schedule around a predetermined structure that may be overly constrained.

Design for a Nominal Flight Condition

For AFCS designs, tight speed control is important in windshear conditions, especially at low altitudes. For this reason, the landing approach condition FLT1 was considered most important and the inner-loop gains were first optimized to give best performance at this flight condition.

Selection of the design parameters for optimization was accomplished with the procedure described in the previous section. The resulting locally optimal design gains are given in Table 3. Current TECS designs are also included in Table 3 for comparison. Notice that the proportional gain K_{TP} is no longer zero.

Closed-loop poles (Table 4) satisfy the desired damping requirements of 0.7, exceeding those obtained by the classical design. Gains in the pitch damper have been reduced, whereas those in the proportional and integral paths to the elevator are

Table 3 Inner-loop and pitch damper feedback gains for flight condition FLT1

Design parameter	Classical design	Optimal design	Optimal design[a]
K_{TP}	0.0	0.111	0.1319
K_{EP}	3.36	3.2682	3.3054
K_{TI}	0.4	0.3603	0.3759
K_{EI}	2.52	2.2428	2.2542
K_q	4.0	3.010	3.0402
K_θ	6.0	3.268	3.4194
k_1	0.9437	0.9142	0.9133
k_2	1.123	−0.1039	−0.0691

[a]Design with additional constraint $E[V^2] \le 0.503816$ fps^2.

increased for improved command bandwidth and tracking performance. With lower pitch damper gains, the bandwidth of the elevator control loop is also reduced. Table 5 summarizes the command and broken-loop control bandwidths for both the optimized and current TECS designs. Notice that the command bandwidths are improved over the classical design with lower control bandwidths.

Table 6 shows closed-loop rms responses of both designs to clear air Dryden turbulence with $\sigma_u = 6.6$ fps and $\sigma_w = 6.3$ fps. Improvement in control rms activity in response to turbulence was accomplished with nonlinear constraints on the respective output covariances, as defined in Eqs. (22) and (23). Notice that the rms response of the speed variable V is slightly higher than that of the classical design. To reduce this response, an additional output covariance constraint is placed on the speed variable as

$$E[V^2] \leq 0.503816 \text{ fps}^2 \tag{28}$$

resulting in a slightly different optimal design (designated in the table). All aircraft covariance responses to clear air turbulence now fall below those of the classical design (Table 6) and the feedback gains are shown in Table 3.

Guaranteed stability margins in the control actuator and sensor paths are shown in Table 7. Results of the optimal and classical designs are comparable.

Table 4 Closed-loop system poles for flight condition FLT1

	Classical design		Optimal design		Optimal design[a]	
Mode	ζ	ω_n, rad/s	ζ	ω_n, rad/s	ζ	ω_n, rad/s
Phugoid	0.64	0.61	0.7	0.78	0.7	0.77
Short period	0.79	3.01	0.7	2.25	0.7	2.33

[a]Design with additional constraint $E[V^2] \leq 0.503816$ fps^2.

Table 5 Command and broken-loop control bandwidths for flight condition FLT1

	Bandwidth, rad/s		
Command/control path	Classical design	Optimal design	Optimal design[a]
γ_c	1.0	1.0	1.0
$\dot{V}_c$	0.8	1.0	1.0
δ_{ec}	4.3	3.3	3.3
δ_{thc}	0.37	0.35	0.36

[a]Design with additional constraint $E[V^2] \leq 0.503816$ fps^2.

Table 6 Closed-loop rms responses to turbulence ($\sigma_u = 6.6$ fps, $\sigma_w = 6.3$ fps) for flight condition FLT1

Variable	Classical design	Optimal design	Optimal design[a]
γ, deg	1.045	0.9224	0.9166
V, fps	0.7098	0.7491	0.7098
n_{zcg}, g	0.0801	0.07983	0.07962
δ_{thc}, lbt/lbw	0.02725	0.02579	0.02596
δ_{ec}, deg	1.4877	1.4585	1.4585

[a]Design with additional constraint $E[V^2] \leq 0.503816$ fps^2.

Gain Schedule Design

Gain schedule of the inner loops is required in order to satisfy design requirements at the cruise condition FLT2. This is accomplished by optimizing the gains K_{GW} and K_{CAS} in the throttle and elevator paths, respectively (Fig. 1). The proportional, integral, and pitch damper gains are fixed at the values optimized for the landing approach condition FLT1. Another set of design objectives is established for the cruise condition similar in form to that given by Eqs. (20-26). They are

1) Stability of the closed-loop eigenvalues:

a) Real parts of all the eigenvalues are restricted to be less than zero, i.e.,

$$\sigma_i < 0, \qquad i = 1,n \tag{29}$$

b) Damping ratios of all the eigenvalues are restricted to be greater than 0.6, i.e.,

$$\zeta_i \geq 0.6, \qquad i = 1,n \tag{30}$$

2) Mean-square responses of control activity to clear air Dryden turbulence of $\sigma_u = 4.7$ fps and $\sigma_w = 4.7$ fps:

$$E[\delta_{thc}^2] \leq 3.2 \times 10^{-5} \text{ (lbt/lbw)}^2 \tag{31}$$

$$E[\delta_{ec}^2] \leq 10.4 \text{ deg}^2 \tag{32}$$

3) Command frequency response bandwidths and command tracking performance:

$$J_1 = \lim_{t_f \to \infty} \frac{1}{2} \int_0^{t_f} E\{Q_1[\gamma(t) - \gamma_c(t)]^2 + Q_2[V(t) - V_c^*(t)]^2\}\, dt \tag{33}$$

The performance index J_1 is evaluated for parameterized random filtered step commands $\dot{V}_c(t)$ and $\gamma_c(t)$ with $\dot{V}_c(t) = V_{co} a e^{-at} \mu(t)$ and $\gamma_c(t) = \gamma_{co}(1 - e^{-at})\mu(t)$, where $\mu(t)$ is the unit step function. The parameter a determines the bandwidths of both the acceleration and the flight-path commands. Again we use $a = 1.2$ rad/s. The variables V_{co} and γ_{co} are random parameters with zero means and covariances $E[V_{co}^2] = \sigma_{V_c}^2 = 1.0$ fps^2 and $E[\gamma_{co}^2] = \sigma_{\gamma_c}^2 = 1.0$ deg^2.

4) Broken-loop crossover frequencies in the control paths:

a) *Throttle control loop*. Control bandwidth of the throttle loop is defined through the performance index

$$J_2 = \lim_{t_f \to \infty} \tfrac{1}{2} E[R_1 \delta_{thc}^2(t_f)] \tag{34}$$

The performance index J_2 is evaluated to a high-pass noise input in the thrust command loop. Cutoff frequency of the high-pass filter is again set approximately equal to the desired broken-loop throttle control bandwidth (i.e., $\omega_{thc} = 0.2$ rad/s).

b) *Elevator control loop*. Similarly, control bandwidth of the elevator loop is defined by

$$J_3 = \lim_{t_f \to \infty} \tfrac{1}{2} E[R_2 \delta_{ec}^2(t_f)] \tag{35}$$

In this case, the performance index J_3 is evaluated to a high-pass noise input in the elevator command loop. Cutoff frequency of the high-pass filter is also set approximately equal

Table 7 Stability margins for flight condition FLT1

	Classical design		Optimal design		Optimal design[a]	
	Gain margin, dB	Phase margin, deg	Gain margin, dB	Phase margin, deg	Gain margin, dB	Phase margin, deg
Actuator paths	$-40, +32$	$+57$	$-35, +\infty$	$+60$	$-38, +\infty$	$+59$
Sensor paths	$-17, +20$	$-70, +63$	$-15, 14$	$-63, +65$	$-16, 14$	$-64, +64$

[a]Design with additional constraint $E[V^2] \leq 0.503816$ fps^2.

to the desired broken-loop elevator control bandwidth (i.e., $\omega_{ec} = 2.0$ rad/s).

Equations (29-35) define individual design requirements for flight condition FLT2. The gain schedule parameters K_{GW} and K_{CAS} along with k_1 and k_2 are then optimized with respect to a single quadratic performance index J of the form

$$J = \sum_{i=1}^{3} W_{pi} J_i \tag{36}$$

subject to the constraints of Eqs. (29-32), where J_i ($i = 1,3$) are defined in Eqs. (33-35). Results of the design optimization are shown in Table 8.

At this flight condition, the optimized gain schedule is quite different from the one chosen in the classical design. Classical design procedures for the selection of the gain schedule are based mostly on closed-loop stability. They may not consider other design objectives such as tracking performance and control response to turbulence. Table 9 shows damping ratios and natural frequencies of the closed-loop system eigenvalues. Minimum damping of 0.6 is achieved in the optimal design through the use of nonlinear constraints in Eq. (30). The results are improved over the closed-loop damping of 0.45 in the classical design. It is also found that a minimum damping requirement of 0.7 on all system modes cannot be achieved with simple gain scheduling of parameters K_{GW} and K_{CAS}. Additional degrees of freedom in the gain schedule parameters are needed (e.g., scheduling of the pitch damper gains K_q and K_θ).

Command and control loop bandwidths are summarized in Table 10. Bandwidths in the acceleration and flight-path command loops are made nearly equal in the optimal design through adjustment of the weighting parameters Q_1 and Q_2 in the cost function J_1 of Eq. (33). Command bandwidths in the classical design are not equal, thus resulting in a less coordinated response to commands. The throttle control bandwidth is reduced significantly in the optimal design; however, this result comes at the expense of an increased bandwidth in the elevator control path. The increase in elevator control bandwidth does not necessarily mean increased elevator activity in turbulence, as seen in Table 11. This design illustrates the benefit of control covariance constraints in maintaining low control activities, while control bandwidths are optimized (i.e., increased) for improved stability of the longitudinal modes.

Closed-loop rms responses to clear air Dryden turbulence are given in Table 11. Control rms responses are maintained at the same level as those of the classical design through nonlinear inequality bounds defined in Eqs. (31) and (32). The results indicate that the optimal design possesses significantly lower throttle activities. Similiar rms elevator control activity is maintained despite higher control bandwidth (Table 10).

Guaranteed stability margins are found to be satisfactory for both the classical and optimal gain schedules. The results are summarized in Table 12.

Conclusions

In this paper, a design method for robust controller design has been applied successfully to the design of an integrated autothrottle/autopilot control system. Much has been learned in the process of formulating a sensible optimal output feedback control problem with solutions comparable to, if not improved over, those achieved using classical single-loop methods. Our formulation of the performance index for command tracking enables designers to identify and even specify the levels of coupling at steady state between aircraft velocity and commands in velocity and flight path. It is found that integral action can only be effective to commands/disturbances with nonzero steady-state values. Closed-loop stability of the short-period and phugoid modes are conveniently achieved through the use of eigenvalue constraints. Control activities in turbulence can be limited directly using covariance constraints. In summary, a systematic procedure has been presented that addresses design issues common to flight control problems, such as closed-loop stability, command tracking performance and bandwidths, and control responses to turbulence. This design framework, based on constrained optimization, will lead to improved design with less guesswork, and allow designers to explore further the potential of a fully integrated design through simultaneous adjustment of the design gains in a multiloop system.

Table 8 Inner-loop gain schedule and design parameters

	FLT1		FLT2	
Parameter	Classical design	Optimal design	Classical design	Optimal design
K_{CAS}	0.9322	0.9322	0.07006	0.1972
K_{GW}	80,000	80,000	80,000	59,352
k_1	0.9437	0.9133	0.9716	0.9769
k_2	1.123	−0.0691	0.1795	−0.3691

Table 9 Closed-loop system poles for flight condition FLT2

	Classical design		Optimal design	
Mode	ζ	ω_n, rad/s	ζ	ω_n, rad/s
Phugoid	0.45	0.42	0.6	0.62
Short period	0.47	3.43	0.68	3.96

Table 10 Command and broken-loop control bandwidths for flight condition FLT2

	Bandwidth, rad/s	
Command/control path	Classical design	Optimal design
γ_c	0.9	0.8
$\dot{V}_c$	0.63	0.75
δ_{ec}	2.7	4.2
δ_{thc}	0.4	0.27

Table 11 Closed-loop rms responses to turbulence ($\sigma_u = 4.7$ fps, $\sigma_w = 4.7$ fps) for flight condition FLT2

Variable	Classical design	Optimal design
γ, deg	0.2810	0.2128
V, fps	0.2792	0.1465
n_{zcg}, g	0.1080	0.08552
δ_{thc}, lbt/lbw	0.00570	0.00349
δ_{ec}, deg	3.2322	3.2249

Table 12 Stability margins for flight condition FLT2

	Classical design		Optimal design	
	Gain margin, dB	Phase margin, deg	Gain margin, dB	Phase margin, deg
Actuator paths	−50, +27	+47	−56, +∞	+80
Sensor paths	−∞, +25	−130, +60	−12,21	−105, +72

Acknowledgments

This work was supported by NASA Grant NAG-1-913 and monitored by R. Hueschen and C. Belcastro. The authors would like to thank the reviewers and the associate editor,

Anthony J. Calise, for their valuable comments and suggestions.

References

[1]Stein, G., and Athans, M., "The LQG/LTR Procedure for Multivariable Feedback Control Design," *IEEE Transactions on Automatic Control,* Vol. AC-32, No. 2, pp. 105–114.

[2]Doyle, J. C., and Glover, K., "State-Space Formulae for All Stabilizing Controllers That Satisfy an H^{∞}-Norm Bound and Relations to Risk Sensitivity," *Systems and Control Letters,* Vol. 11, 1988, pp. 167–172.

[3]Doyle, J. C., "Analysis of Feedback Systems with Structured Uncertainties," *IEE Proceedings,* Vol. 129, Pt. D, No. 6, 1982.

[4]Levine, W. S., Johnson, T. L., and Athans, M., "Optimal Limited State Variable Feedback Controllers for Linear Systems," *IEEE Transactions on Automatic Control,* Vol. AC-16, No. 6, pp. 785–793.

[5]Halyo, N., and Broussard, J. R., "Algorithms for the Output Feedback, Multiple Model and Decentralized Control Problems," NASA CP-2296, Oct. 1983.

[6]Ly, U., "A Design Algorithm for Robust Low-Order Controllers," Ph.D. Dissertation, Stanford Univ., Stanford, CA, Nov. 1982.

[7]Ly, U., "A H^2 and H^{∞} Design Tool for Linear Time-Invariant Systems," *Proceedings of the Third Annual Conference on Aerospace Computational Control,* Vol. 1, Jet Propulsion Lab., Pasadena, CA, Pub. 89-45, Aug. 1989, pp. 312–326.

[8]Gill, P. E., Murray, W., Saunders, M. A., and Wright, M. H., "User's Guide for NPSOL (Version 4.0): A Fortran Package for Nonlinear Programming," Stanford Univ., Stanford, CA, Tech. Rept. SOL 86-2, Jan. 1986.

[9]Lambregts, A. A., "Integrated System Design for Flight and Propulsion Control Using Total Energy Principles," AIAA Paper 83-2561, Oct. 1983.

[10]Lambregts, A. A., "Operational Aspects of the Integrated Vertical Flight Path and Speed Control Systems," Society of Automotive Engineers, Warrendale, PA, SAE Paper 83-2239, Aug. 1983.

[11]Lambregts, A. A., "Vertical Flight Path and Speed Control Autopilot Design Using Total Energy Principles," AIAA Paper 83-2239, Aug. 1983.

[12]Bruce, K. R., "Integrated Autopilot/Autothrottle Based on a Total Energy Control Concept: Design and Evaluation of Additional Autopilot Modes," NASA NAS1-16300, Aug. 1987.

[13]Bruce, K. R., "Integrated Autopilot/Autothrottle for the NASA TSRV B-737 Aircraft: Design and Verification by Nonlinear Simulation," NASA CR-4217, Feb. 1989.

[14]Bruce, K. R., Kelley, J. R., and Person, L. H., "NASA B737 Flight Test Results of the Total Energy Control System," AIAA Paper 86-2143, Aug. 1986.

[15]Vinkler, A. P., Wood, L. J., Ly, U., and Cannon, R. H., "Minimum Expected Cost Control of Linear Systems with Uncertain Parameters—Applications to Remotely Piloted Vehicle Flight Control Systems," *Proceedings of the AIAA Guidance and Control Conference,* AIAA, New York, Aug. 1979.

[16]Ly, U., "Optimal Low Order Flight Critical Pitch Augmentation Control Law for a Transport Airplane," *Proceedings of the AIAA Guidance and Control Conference,* AIAA, New York, Aug. 1984, pp. 743–757.

[17]Jones, R. D., Bossi, J., and Ly, U., "Multivariable Regulator Design for Robustness and Performance: A Realistic Example," *Proceedings of the American Control Conference,* Institute of Electrical and Electronics Engineers, June 1986, pp. 285–288.

[18]Rosenthal, D. E., "Experiments in Control of Flexible Structures with Uncertain Parameters," Stanford Univ., Stanford, CA, Rept. SUDAAR 542, March 1984.

[19]Byun, K. K., "Robust Control Synthesis for Uncertain Dynamical Systems," *Proceedings of the AIAA Guidance and Control Conference,* AIAA, Washington, DC, Aug. 1989, pp. 792–801.